

A short peptide synthon for liquid-liquid phase separation

Manzar Abbas^{1,†}, Wojciech P. Lipiński^{1,†}, Karina K. Nakashima¹, Wilhelm T.S. Huck¹ and Evan Spruijt^{1,*}

¹ Institute for Molecules and Materials, Radboud University, Heyendaalseweg 135, 6525 AJ Nijmegen, The Netherlands

[†] These authors contributed equally to the work

* E-mail: e.spruijt@science.ru.nl

Abstract

Liquid-liquid phase separation of disordered proteins has emerged as a ubiquitous route to membraneless compartments in living cells, and similar coacervates may have played a role when the first cells formed. However, existing coacervates are typically made of multiple macromolecular components, and designing short peptide analogues capable of self-coacervation has proven difficult. Here, we present a short peptide synthon for phase separation, made of only two dipeptide stickers linked via a flexible, hydrophilic spacer. These small-molecule compounds self-coacervate into micrometre-sized liquid droplets at sub-mM concentrations, which retain up to 75 weight-% water. The design is general and we derive guidelines for the required sticker hydrophobicity and spacer polarity. To illustrate their potential as protocells, we create a disulphide-linked derivative that undergoes reversible compartmentalisation controlled by redox chemistry. The resulting coacervates sequester and melt nucleic acids, and act as microreactors that catalyse two different anabolic reactions yielding molecules of increasing complexity. This provides a stepping stone for new protocells made of single peptide species.

Introduction

Compartmentalisation is one of the central pillars of living systems and represents a key step in the emergence of life.¹⁻³ To understand how abiotic components could become organised in life-like compartments with the ability to adapt and evolve, various types of protocells have been developed, including giant unilamellar vesicles, oil-in-water droplets, coacervates, and colloidosomes.⁴⁻⁸ Lipid vesicles are commonly seen as one of the most plausible predecessors of modern cells.^{5,8,9} Their architecture strongly resembles the membranes found in all living cells and they can form spontaneously upon hydration from amphiphilic molecules. In addition, they have been shown to grow and split through swelling and physical disruption, respectively,¹⁰ which could be combined into a primitive cell cycle.⁸ However, their lack in permeability to many polar building blocks of for example RNA and peptides poses problems for protometabolism and the flow of molecular information.^{11,12}

Membraneless coacervates are alternative compartments that are not hindered by these limitations.^{6,13} Such compartments are formed spontaneously by liquid-liquid phase separation of mostly macromolecular components, and are able to concentrate a wide range of solutes by partitioning. Contrary to oil droplets, coacervates retain a large amount of water and provide an environment in which ribozymes^{14,15} and enzymes^{16,17} can be active. In recent years, liquid-liquid phase separation has also emerged as a ubiquitous route to the formation of membraneless compartments by partly disordered proteins in living cells.¹⁸⁻²⁰ Their widespread occurrence and central roles suggest that prebiotic analogues of these intracellular condensates could have played a role in the emergence of cells. However, the fact that coacervates are typically made of large molecules and often require multiple interacting components is commonly regarded as a serious barrier for their relevance as protocells.^{6,13} Coacervates made of single nucleotide triphosphates,¹³

short oligonucleotides,²¹ and peptides^{22,23} have been reported, but they still require oppositely charged species of higher molecular weight to form. Designing short peptide-based molecules that are capable of self-coacervation, analogous to disordered proteins undergoing phase separation in living cells such as FUS²⁴ and hnRNPA1,²⁵ has proven difficult. Various motifs and interactions underlying LLPS have been identified,²⁶ but a minimal model system is still lacking.

Here, we present a short peptide synthon for liquid-liquid phase separation. Our design is based on the sticker-spacer motif that was recently identified as an important characteristic of several phase-separating proteins,²⁵ and provides a route to peptide-based protocells through self-coacervation of small molecules. We show that various dimers of aromatic or aliphatic dipeptides, linked by a hydrophilic spacer, can self-coacervate into micrometre-sized liquid droplets at sub-mM concentrations in a wide range of environmental conditions. Unlike previously reported supramolecular assemblies of dipeptides,^{27–30} these coacervate droplets are liquid, reversible, rich in water and responsive to pH, temperature and organic solutes, analogous to many intracellular condensates of disordered proteins. By using a disulphide-containing moiety to connect the dipeptide stickers together, we create versatile coacervate protocells made of a single component that can be formed and dissolved reversibly by controlling the redox chemistry. These coacervate protocells further act as effective microcompartments that can take up a wide range of guests, including single-stranded DNA, RNA porphyrins and various organic dyes. Small RNA hairpins dehybridise upon uptake, while rotationally dynamic dyes such as thioflavins partly lose their rotational freedom inside the coacervates. Finally, we show how these peptide-based coacervates could play a role in the formation of molecules of increasing complexity, by acting as microreactors for different types of addition reactions. An aldol reaction and hydrazone formation occurred 44 and 13-fold faster, respectively, compared to the same reaction in aqueous solution, because of reactant sequestration and the local apolar environment inside the coacervates facilitating the

reactions. These properties make coacervates of disulphide-coupled peptides promising and versatile protocells. The general design presented here could open the way for new protocells made of single peptide species, and model systems to obtain a fundamental insight into intracellular phase separation.

Results

Self-coacervation of peptide derivatives

Aromatic residues are known to be important for the phase separation propensity of disordered proteins.^{24,25,31} Recently, a sticker-spacer motif has been proposed that explains how separating these aromatic residues (stickers) by flexible regions of soluble residues (spacers) results in liquid condensates instead of solid aggregates.²⁵ However, a minimal design for protein liquid-liquid phase separation, which could provide a starting point for single-component coacervate protocells, is still lacking. We hypothesised that linking two hydrophobic dipeptides together with a flexible, polar spacer could result in the formation of condensed liquid droplets if the association between the dipeptides was strong enough. Aromatic dipeptides such as phenylalanyl-phenylalanine (FF) have been widely studied for their ability to self-assemble into fibres and hydrogels.^{27–30} However, these assemblies are often irreversible and do not yield liquid condensates capable of sequestering other solutes. By joining them together through a non-aromatic, flexible linker, a minimal motif consisting of two stickers and a spacer is created that can undergo simple coacervation above a critical association concentration. Similar sticker-spacer motifs have been used in other fields, such as polymer chemistry, to predict self-assembly and phase separation of block copolymers, for example.^{32,33}

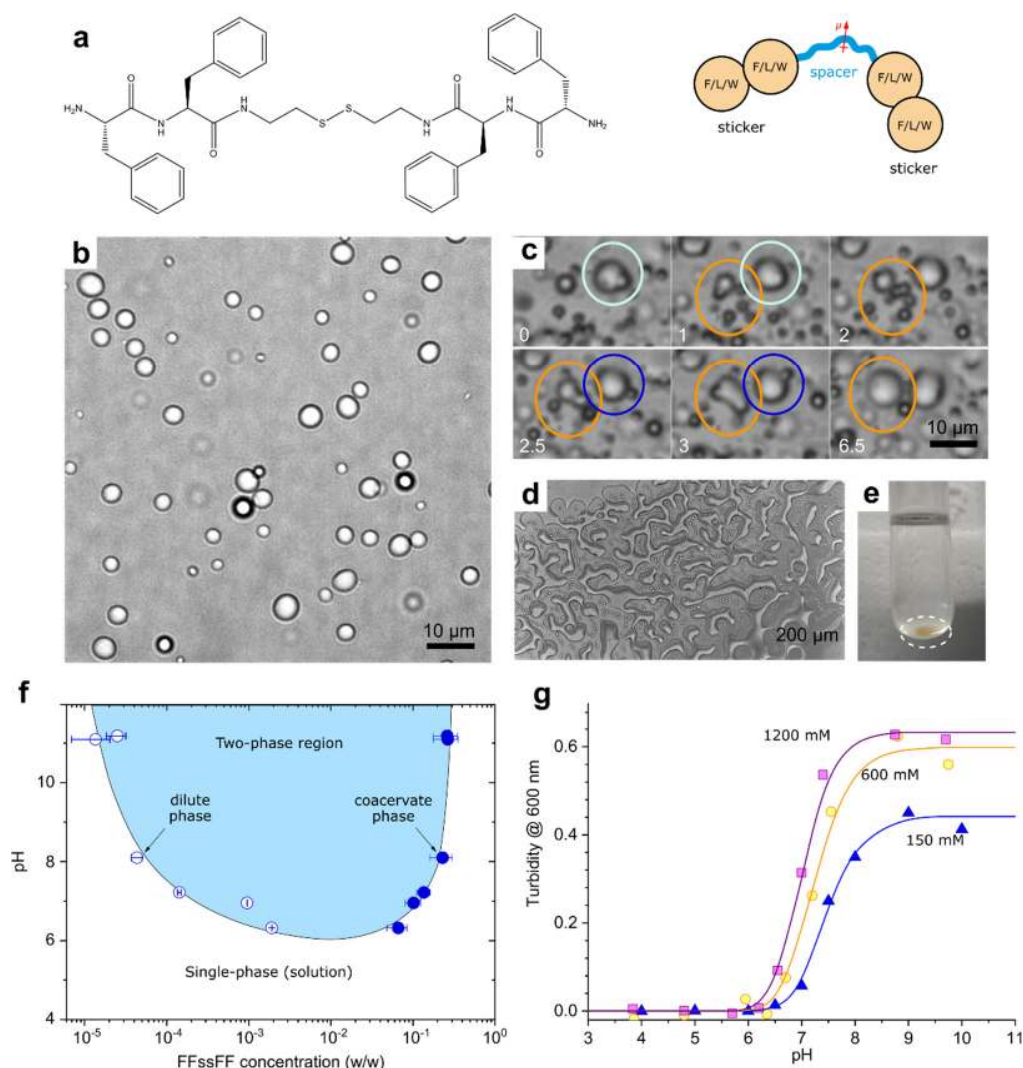


Figure 1: Liquid-liquid phase separation of cystamine-linked phenylalanine dipeptides. (a) Structure of FFssFF and schematic illustration of synthon motif comprising two dipeptide stickers and a polar spacer, (b) microscope image of droplets of FFssFF (1 mg/mL, pH 8) after 5 minutes incubation, (c) fusion of FFssFF coacervate droplets (2 mg/mL, pH 8) (labels indicate time in minutes), (d) wetting patterns formed by FFssFF coacervates (2 mg/mL, pH 8) on a glass surface, (e) bulk coacervate phase collected after centrifugation (3 mg/mL, pH 8, 4,000 rcf), (f) phase diagram of FFssFF coacervation, the shaded area is the two-phase region in which coacervates are formed, error bars indicate the measurement uncertainty in the solution and coacervate masses, (g) pH-triggered phase transition in FFssFF solutions (0.5 mg/mL) at different salt concentrations monitored by turbidity.

In order to create a conjugate that could be used to develop tunable protocells, we selected a cystamine moiety to link two *L*-phenylalanyl-*L*-phenylalanine dipeptides together via their C-termini (Figure 1a). The disulphide bond of this linker allows for dynamic control over the

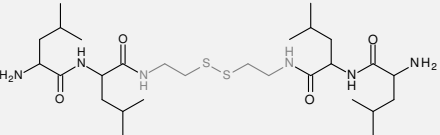
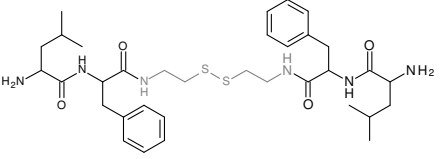
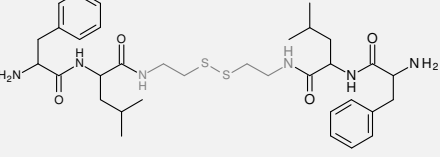
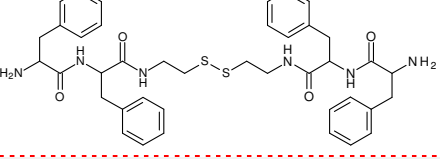
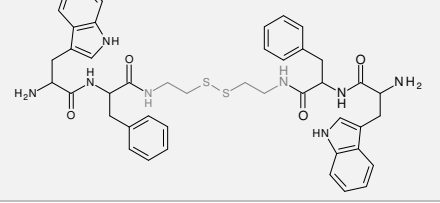
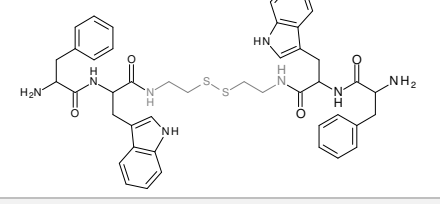
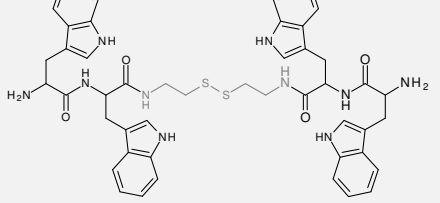
assembly through redox chemistry.³⁴ Contrary to FF dipeptides and most FF derivatives, the cystamine-conjugated derivative bis(phenylalanyl-phenylalanyl)cystamine (FFssFF in short) is completely soluble in water below pH 6 up to 15 mg/mL and no aggregation could be detected (Figure S1). However, when the pH was increased to 7 or higher, the solution of FFssFF became turbid (Figure S2). Microscopic investigation revealed the formation of condensed droplets with a typical size of 1-10 μm (Figure 1b). These peptide-rich condensates are liquid, which is evident from their ability to fuse (Figure 1c), spread and deform (Figure 1d), and ultimately separate into a bulk phase after centrifugation (Figure 1e), just like coacervates of polyelectrolytes or disordered proteins.^{13,22,23}

An important difference between these FFssFF droplets and other coacervates made of polyelectrolytes or proteins is the size of the constituent molecules. While synthetic polymers, RNA and intrinsically disordered proteins used to make coacervate droplets have a typical mass of more than 10 kDa, these peptide derivatives are small molecules with a molecular weight of less than 750 Da. Nonetheless, the droplets shown in Figures 1 and S1 are coacervates: they are condensed liquids containing the same solvent as the coexisting dilute phase (water) and enriched in at least one of the dissolved species (FFssFF).³⁵ We determined the amount of water present in the coacervate droplets by separating them from the supernatant after centrifugation (Figure 1e), and found that they indeed contain a significant amount of water ($75 \pm 10\%$ (w/w) at high pH). In addition, the droplets contain a very high peptide concentration, reaching 1,000-fold higher concentrations than the surrounding dilute solution (Figure 1f). Because of the high internal concentration, coacervates of FFssFF do not coalesce easily, and the average droplet size of an emulsion of FFssFF coacervates increases only slowly over time (Figure S3). Eventually, the coacervates droplets undergo complete fusion, indicating that the peptides remain sufficiently mobile.

A second difference between FFssFF coacervates and most other coacervate protocells studied so far, is that these types of peptide coacervates designed with a sticker-spacer architecture do not require combining two oppositely charged species.^{13,22,23} The droplets shown in Figure 1 form as a result of self-interaction between the apolar side groups of FFssFF (Figure S4-6), and are therefore called simple coacervates.³⁶ Measurements of FFssFF coacervation at different salt concentrations confirm that the ionic strength has a very small effect on the coacervation transition (Figure 1g) and coacervate stability (Figure S7), while the phase transition is sensitive to temperature and organic solutes (Figure S5-6). This situation is similar to the phase separation of aromatic-rich disordered proteins like FUS²⁴ and hnRNPA1,²⁵ and the design shown in Figure 1a could be regarded as a minimal sticker-spacer motif required for phase separation. In contrast, the FFssFF coacervates are fundamentally different from oil droplets in water that have been studied as protocell models,^{37,38} even though hydrophobic interactions underlie the formation of both. Coacervates, like the FFssFF droplets in Figure 1, constitute a liquid phase that contains both peptides and water, which only exists when the peptide is dissolved in water. This situation is analogous to the formation of membraneless organelles from hydrated disordered proteins.

To explore the general nature of the design in Figure 1a, we synthesised variants with different hydrophobic dipeptides (stickers, Table 1) and different hydrophilic linkers (spacers, Table 2), including a cystine linker. Compounds with amino acids carrying less hydrophobic side chains like leucine ($\Delta G_{w-oct} = -5.2$ kJ/mol versus -7.1 for phenylalanine) formed clear liquid coacervate droplets, but required higher concentrations (Table 1, Figure S8). Mixed compounds (FLssLF and LFssFL) had a critical coacervation concentration between the homodipeptide compounds LLssLL and FFssFF. For compounds with more hydrophobic side chains like tryptophan ($\Delta G_{w-oct} = -8.7$ kJ/mol) the associations became too strong, and solid aggregates were

Table 1: Self-coacervation of different hydrophobic dipeptide stickers connected with a disulphide spacer. The red dashed line highlights the boundary between compounds forming aggregates and coacervates, located at a threshold sticker hydrophobicity expressed by the water-octanol transfer free energy.

Sticker	Structure	Condensate appearance	$\Delta G_{w-oct, sticker}$ (kJ/mol) ^{a)}	Saturation concentration (mg/mL) ^{b)}	Partitioning coefficient ThT ^{c)}
LL		coacervate	-10.4	2.1	18
LF		coacervate	-12.3	0.054	6.3
FL		coacervate	-12.3	0.066	9.1
FF		coacervate	-14.2	0.018	30
WF		aggregate	-15.8	0.002	n.d.
FW		aggregate	-15.8	0.002	n.d.
WW		aggregate	-17.4	0.001	n.d.

^{a)} Calculated as the sum of amino acid side chain transfer free energies
^{b)} HPLC analysis
^{c)} Confocal fluorescence microscopy analysis

Table 2: Self-coacervation of FF dipeptide stickers connected with different linkers. The red dashed line highlights the boundary between compounds forming aggregates and coacervates, coinciding with a zero or negative solvation free energy and an increase in dipole moment. Error bars correspond to standard deviations of six calculations.

Spacer	Structure	Condensate appearance	Spacer solubility (mg/mL) ^{a)}	$\Delta G_{\text{solv, spacer}}$ (kJ/mol) ^{b)}	Dipole moment (D) ^{b)}	Saturation concentration (mg/mL) ^{c)}	Partitioning coefficient ThT ^{d)}
CC		aggregate	0.12	18 ± 1.3	0.2 ± 0.2	n.d.	n.d.
CC ^{e)}		aggregate	0.12	18 ± 1.3	0.2 ± 0.2	n.d.	n.d.
c6		aggregate	0.49	11 ± 2.0	2.0 ± 0.7	0.06	n.d.
c8		aggregate	0.58	19 ± 1.2	1.9 ± 0.9	0.006	n.d.
c6(Me)₃ ^{f)}		aggregate / gel-like	>100	17 ± 1.6	2.2 ± 0.8	0.016	n.d.
ss		coacervate	>100	-12 ± 6.0	4.8 ± 0.8	0.018	30
s		coacervate	>100	-8.0 ± 3.1	3.3 ± 1.1	0.097	24
o		coacervate	>100	-0.4 ± 2.8	2.9 ± 0.8	0.18	12.8
eo₂ ^{f)}		coacervate	>100	0.9 ± 2.4	2.8 ± 0.7	0.45	9.3

^{a)} Information provided by supplier.
^{b)} PM3 calculations using MolCalc (see Supplementary Methods).
^{c)} HPLC analysis
^{d)} Confocal fluorescence microscopy analysis.
^{e)} Phenylalanylphenylalanine (FF) linked via N-terminus
^{f)} Mixture of stereoisomers

found for WWssWW and the mixed compounds WFssFW and FWssWF. All liquid coacervates could take up the hydrophobic dye thioflavin-T (ThT) by partitioning.

Analysis of the condensation of different spacers revealed that polar and unstructured spacers with heteroatoms were all able to form coacervates (Table 2, Figure S9). With the apolar 1,6-hexanediamine spacer, only aggregates were observed, while 2,2,4(2,4,4)-trimethyl-1,6-hexanediamine appeared to be at the boundary between coacervate and aggregate, showing tiny solvated globules attached together in a fractal-like aggregate (Table 2, Figure S9I). Taking the spacer's free energy of solvation and dipole moment as indicators of their ability to solubilise the stickers and keep the condensates in a hydrated, liquid state, we find a clear boundary between

polar spacers with a zero or negative solvation free energy, which give rise to coacervates, and apolar spacers with a positive solvation free energy and limited solubility, which give rise to aggregates (Table 2). Finally, compounds with a cystine spacer did not form coacervates, in agreement with cystine's low solubility and the propensity of cystine-containing peptides to form highly structured aggregates through β -sheet hydrogen bonding.³⁹ These guiding principles suggest that in the case of a motif with a polar spacer and stickers that are just not hydrophobic enough, for instance because the pH is too low, phase separation could be induced by changing the solvent polarity. This is indeed what we observe for FFssFF solutions at pH 6.8 by increasing the salt concentration (Figure 1g). In brief, hydrophobic dipeptide stickers linked by an unstructured, polar spacer are minimal motifs for simple coacervation.

Redox reversibility of coacervation

We selected the phenylalanyl-phenylalanine peptide derivatives with a cystamine linker (FFssFF) to investigate the properties that make these coacervates attractive protocells in more detail. The disulphide bond allows direct control over coacervate formation by redox chemistry. By reducing the disulphide bond in FFssFF with tris(2-carboxyethyl)phosphine (TCEP), the peptide derivative is converted in two free thiols that are soluble in water, even at pH > 7, and a turbid dispersion of coacervate droplets is converted into a clear solution (Figure 2a). This transition is completely reversible by oxidation of the free thiols using oxidizing agents (Figure 2a,b).

We monitored the redox-controlled phase transition in more detail using a turbidity titration. Figure 2c shows the complete disappearance of turbidity in a 1.0 mg/mL dispersion of FFssFF coacervates within 10 minutes upon addition of 18 mM TCEP. Mass spectrometry confirmed that all disulphides had been reduced to free FF-SH (Figure S10b,e). Subsequent addition of 70 mM of $K_3Fe(CN)_6$ resulted in the formation of identical liquid droplets as before

reduction (Figure 2c) and reappearance of turbidity over 15 minutes. Mass spectrometry confirmed the formation of the original FFssFF (Figure S10c,f). These regenerated coacervates could be completely dissolved again by reduction with TCEP, indicating that they have the same redox sensitivity as the originally formed coacervates. The turbidity after oxidation did not reach the same level as before the first reduction, because the rate of coacervation is different. Initially, coacervates were formed very rapidly, within seconds, by increasing the pH of an acidic solution of FFssFF to 7. Coacervation by oxidation of thiols takes significantly longer and some coacervates could have settled and adhered to the walls of the measuring chamber during that time. The same phenomenon is also observed when the turbidity decreases immediately after switching the pH (Figure 2c,d).

The redox-induced coacervation is not limited to TCEP and ferricyanide. Any sufficiently strong reducing and oxidizing agent can drive the conversion. We carried out the same turbidity

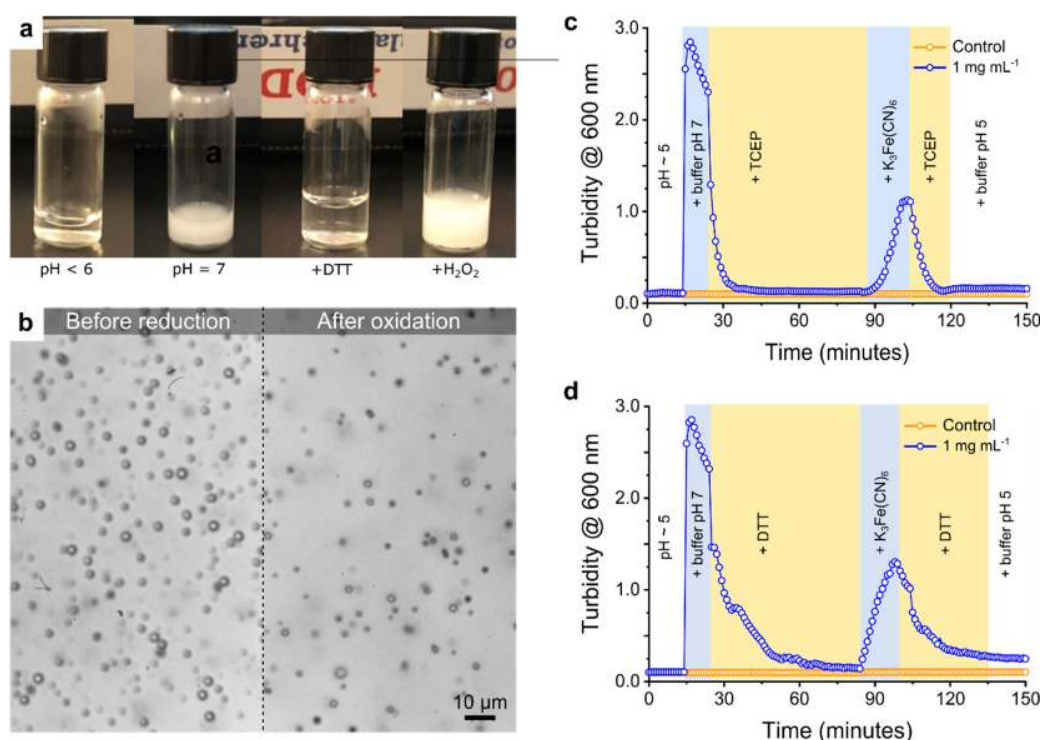


Figure 2: Reversible reduction and oxidation of FFssFF. (a) Pictures of FFssFF under different conditions, (b) FFssFF coacervate droplets before reduction and after oxidation, (c) kinetics of dissolution of FFssFF coacervates upon reduction with TCEP, and formation of coacervates through condensation upon oxidation with K₃Fe(CN)₆, as monitored by turbidity, (d) same as (c) using DTT as reducing agent.

titration carried out with DTT as reducing agent (Figure 2d) and hydrogen peroxide as oxidizing agent (Figure S11), and found the same behaviour in both cases. These results show that oxidation of small dipeptide-conjugated thiols, such as FF-SH, under prebiotically relevant conditions can result in the efficient and spontaneous formation of protocellular compartments.

Selective partitioning of RNA, DNA and small molecule guests

One of the most important characteristics of coacervates and an argument for their potential relevance in the emergence of life is their ability to take up a wide variety of guest molecules and concentrate them to potentially high enough concentrations to facilitate reactions.^{6,13,17} We determined the ability of the FFssFF coacervates to concentrate different guest molecules by fluorescence microscopy, as shown in Figure 3. Aromatic fluorophores, including thioflavin T (ThT, Figure 3a-b), 4',6-diamidino-2-phenylindole (Dapi, Figure 3c), methylene blue (Figure 3d) and SYBR Green (Figure 3f) all became strongly concentrated inside FFssFF coacervates, with apparent partition coefficients ($K=c_{\text{droplet}}/c_{\text{solution}}$) of 30, 35, 21, and 56, respectively. In the case of ThT, the strong fluorescence suggests that this fluorophore becomes rotationally restricted inside the coacervates by binding to the apolar peptide side groups, similar to its binding to beta sheet structures in proteins. The fluorescence intensity of ThT in LLssLL coacervates was slightly lower ($K=18$, Figure S12), as expected based on the weaker preference of ThT for the aliphatic isobutyl side chains of leucine.⁴⁰ Fluorescein was also taken up and concentrated inside FFssFF coacervates but to a much smaller extent (Figure 3e, $K=1.7$). We attribute this to fluorescein's strongly hydrated negative charges at pH 7, which have little association with the coacervate components.

Apart from small molecule fluorophores, these peptide-based coacervates also sequester longer nucleic acids. Figures 3g and 3h show fluorescence microscope images of FFssFF coacervates that were incubated with 500 nM of and RNA (24 nt), respectively. Both nucleic acids

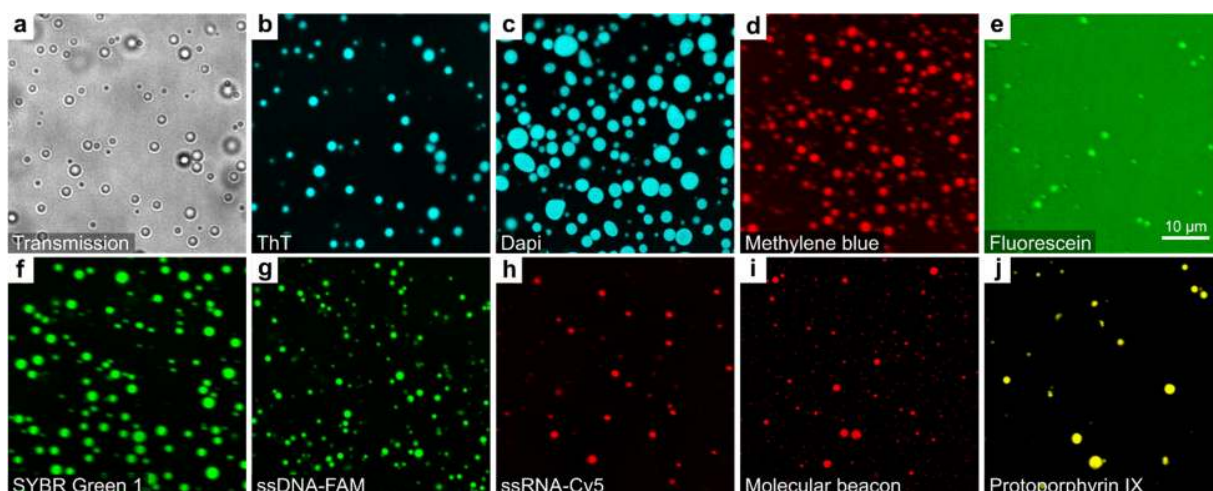


Figure 3: Partitioning of guest molecules in FFssFF coacervates. (a) Brightfield image of FFssFF coacervates incubated with ThT, (b) confocal fluorescence image of ThT at the same position, (c) confocal fluorescence image of FFssFF coacervates incubated with Dapi, (d) same for methylene blue, (e) same for 5(6)-carboxyfluorescein, (f) same for SYBR Green I, (g) same for fluorescein amine-labelled ssDNA (43 nt), (h) same for Cy5-labelled ssRNA (24 nt), (i) same for RNA molecular beacon, and (j) same for protoporphyrin IX. The scale bar is shown in panel (e) and is the same for all images.

are distributed homogeneously in the coacervate droplets ($K=68$ and 75 , respectively) and their partitioning is most likely dominated by favourable base-stacking interactions between the FFssFF and the nucleotide bases, while the phosphate charge plays only a minor role. We asked whether these peptide coacervates could have the same dehybridizing effect on nucleic acid duplexes as analogous condensates formed by disordered proteins.⁴¹ We incubated the coacervates with a short RNA hairpin with a 4 bp GC-stem designed to melt at 53°C (50 mM NaCl, pH 7.4) and functionalised with a fluorophore-quencher pair.⁴² We found that the hairpin was taken up and melted in the FFssFF coacervates (Figure 3i), evidenced by the strong fluorescence signal compared to a control with 10-fold higher concentration of the same hairpin in buffer (Figure S13). Finally, also protoporphyrin IX, a prototypical tetrapyrrole macrocycle and a precursor for hemoglobin and chlorophyll, was concentrated in the FFssFF coacervates (Figure 3j, $K=35$).

Enhanced rates of addition reactions in coacervate protocells

Inspired by the partitioning of both small molecules and large nucleic acids in FFssFF coacervates, we set out to investigate if they could act as microreactors and enhance anabolic reactions yielding molecules of increasing complexity. First, we investigated the aldol reaction of an enol and an aldehyde, leading to C-C bond formation (Figure 4a). This reaction is generally slow at neutral pH, but is known to be catalysed by proline and by various dipeptides,⁴³ though it typically proceeds at appreciable rate only if one of the substrates is added in large excess. Aldol reactions play an important role in the synthesis of sugars, in the Krebs's cycle, and in various other protometabolic cycles.⁴⁴ We selected *p*-nitrobenzaldehyde (PNB) and cyclohexanone (CH) to enable monitoring the reaction kinetics by ¹H NMR. Without coacervates, no significant decrease in aldehyde concentration was observed in 48 hours. Fitting of the integrated NMR data to a first-order rate equation for the aldehyde gave an apparent rate constant of $1.1 \pm 0.26 \cdot 10^{-3} \text{ h}^{-1}$. By contrast, in the presence of FFssFF coacervates, complete disappearance of the aldehyde peak and formation of the aldol product was observed in approximately 48 hours, with an apparent rate constant of $46 \pm 1.0 \cdot 10^{-3} \text{ h}^{-1}$ (Figure 4a). In a control reaction with peptides but without coacervates, no conversion was observed in 48 h (Figure S14), suggesting that the dipeptides alone do not catalyse the reaction sufficiently to observe complete conversion at the concentrations we used.

This 44-fold rate enhancement can thus be explained by concentration of the reactants inside the coacervates or the local apolar environment affecting the reaction barrier, or a combination of both, analogous to the rate enhancement in single-chain polymer nanoparticles.⁴⁵ When we performed a control reaction with tenfold higher concentration of both reactants, we did not observe any significant conversion (Figure S15), and the apparent rate constant of $2.1 \pm 0.41 \cdot 10^{-3} \text{ h}^{-1}$ was still far from the observed rate in coacervates. We estimated the partitioning coefficients of PNB by absorbance, and found that it partitions only weakly in FFssFF coacervates ($K=3.5$), as

expected for a small molecule. We therefore conclude that a significant part of the rate enhancement is the result of the local (hydrophobic) environment in the FFssFF coacervates that facilitates the aldol reaction, like in catalysis, with an estimated decrease of the reaction energy barrier of 6.3 kJ/mol.

We then looked at the hydrazone formation reaction between an aldehyde and a hydrazine, which is also slow at neutral pH without catalyst.⁴⁶ This reaction provides an effective way to form C-N bonds and is frequently used in dynamic combinatorial chemistry to create libraries of many possible conjugation products. We incubated 1 mM *p*-nitrobenzaldehyde and 0.2 mM phenyl hydrazine in the absence and presence of FFssFF coacervates at room temperature, pH 7 (Figure 4b). The hydrazone product of this reaction exhibits a clear absorption band at 421 nm,⁴⁷ and its formation was confirmed by HPLC (Figure 4b-v, and Figure S16). We fitted the increase in absorbance to a first-order rate equation and found an apparent rate constant of $0.11 \pm 0.02 \text{ h}^{-1}$ for the reaction without coacervates, and $1.4 \pm 0.17 \text{ h}^{-1}$ in the presence of coacervates, a 12-fold enhancement. Like for the aldol reaction, this enhancement is explained by a combination of reactant concentration and the local apolar environment that facilitates condensation. Concentration of the reactants alone does not account for the observed rate enhancement: the partition coefficient of PH ($K=1.8$) is even lower than PNB ($K=3.5$), and when we repeated the experiment with fivefold higher concentrations of both the aldehyde and hydrazine, we observed an apparent rate constant of $0.69 \pm 0.11 \text{ h}^{-1}$ (Figure S17), which is still more than twofold lower than inside the coacervates. The reaction barrier for hydrazone formation is thus lowered by 1.6 kJ/mol inside the FFssFF coacervate protocells, and these compartments could be seen as catalytic microreactors for both reactions.

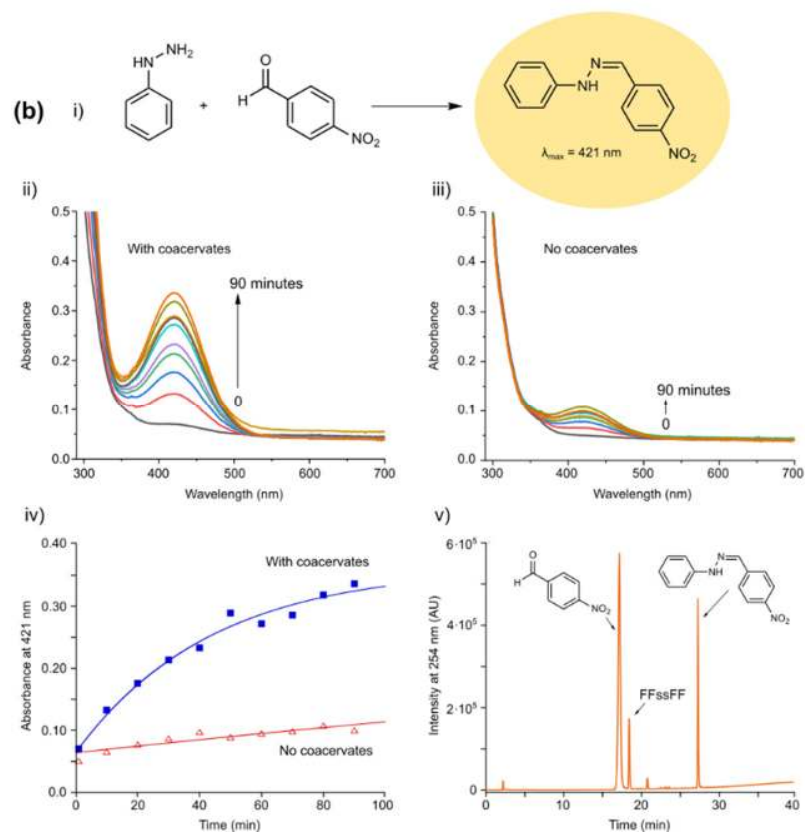
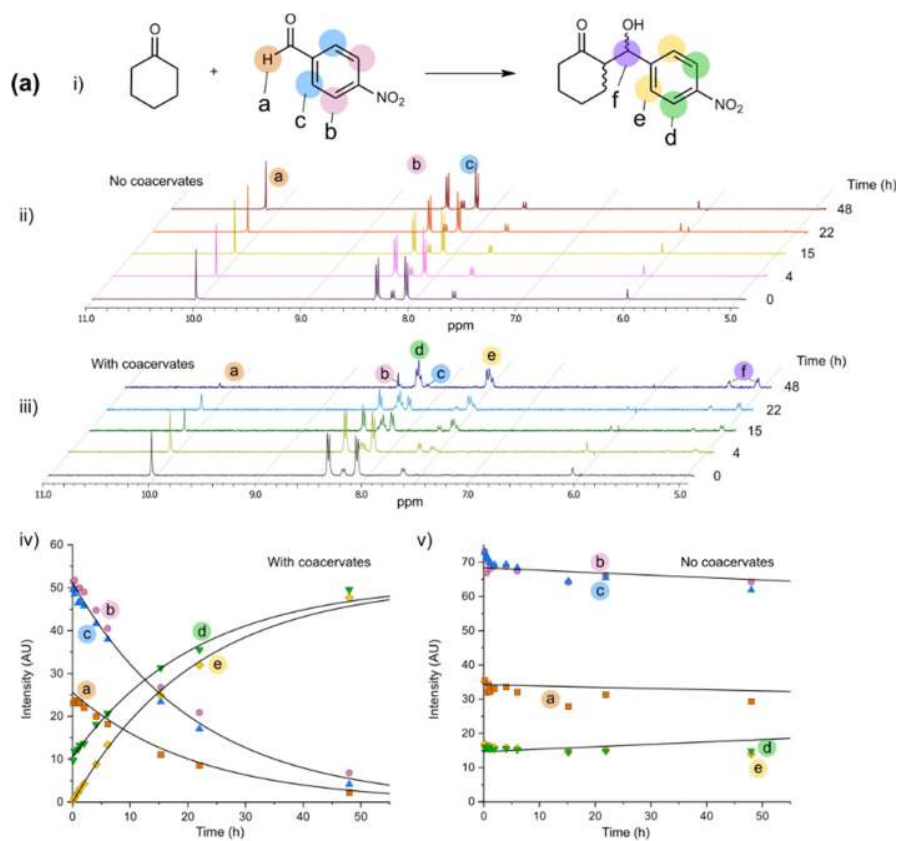


Figure 4: Enhanced rates of addition reactions in FFssFF coacervates. (a) Aldol reaction between cyclohexanone and *p*-nitrobenzaldehyde. i) Reaction scheme, ii) ¹H-NMR spectra of the reaction mixture without coacervates taken after different incubation times, iii) same as ii) but with FFssFF coacervates (peptide concentration 0.2 mg/mL). Characteristic peaks are indicated by labels a-f. iv) Kinetics of aldol reaction in the presence of coacervates, as monitored by NMR. Solid lines are simultaneous fits to all data using a first-order rate equation. v) same as iv) for the reaction without coacervates. (b) Hydrazone formation between phenylhydrazine and *p*-nitrobenzaldehyde. i) Reaction scheme, ii) UV-Vis spectra of the reaction mixture with FFssFF coacervates taken after different incubation times (peptide concentration 0.2 mg/mL), iii) same as ii) but without coacervates. iv) Kinetics of hydrazone formation in the presence and absence of coacervates. Solid lines are simultaneous fits to both data using a first-order rate equation with variable rate constant. v) HPLC analysis of the reaction mixture with coacervates after 90 minutes, showing peaks for the reactants and the product.

Conclusions

We have developed a new class of short peptide derivatives, which represent a synthon for liquid-liquid phase separation. When dissolved in water, these small-molecule compounds self-coacervate into stable liquid droplets that contain up to 75 wt-% water, upon increasing the temperature or pH. The peptide derivatives were designed after a recent sticker-spacer model for protein phase separation²⁵ and represent the minimal motif required for phase separation. The derivatives consist of two hydrophobic dipeptide stickers, linked together by a flexible hydrophilic spacer. We have identified guidelines for sticker hydrophobicity and spacer polarity that define the boundary between dynamic liquids and aggregated solids. For intracellular protein condensates, precisely this boundary is believed to separate healthy organelles from disease states,¹⁹ and the minimal LLPS motif presented here could open the way for the development of model systems to systematically study the molecular principles underlying the liquid-to-solid transition. An important first step would be to use bioinformatics tools and computer-aided peptide design to identify minimal unstructured peptide sequences to replace the pseudopeptide linker in our synthon.⁴⁸

Moreover, the minimal sticker-spacer coacervates we created are attractive protocell models, based on their structural simplicity and unique chemical properties. We have used FFssFF,

a disulphide-linked derivative with two aromatic dipeptides to show for the first time that a single small-molecule compound can form effective microcompartments by self-coacervation at sub-mM concentrations. We were able to control the formation of these protocells using redox chemistry, and to sequester and melt nucleic acids inside these coacervates. Finally, the coacervates can act as catalytic microreactors for two widely used addition reactions. The rate enhancement of aldol and hydrazone formation reaction can only be explained by a combination of increased concentration and a lowering of the reaction barrier due to the local apolar environment, similar to what happens in micellar catalysis.⁴⁹ These results are a proof of principle of coacervate catalysis, and provide a stepping stone for the development of a wide range of new protocells with catalytic properties made of single peptide species.

References

1. Koshland Jr., D. E. SPECIAL ESSAY: The Seven Pillars of Life. *Science* **295**, 2215–2216 (2002).
2. Yewdall, N. A., Mason, A. F. & van Hest, J. C. M. The hallmarks of living systems: towards creating artificial cells. *Interface Focus* **8**, 20180023 (2018).
3. Mann, S. Systems of Creation: The Emergence of Life from Nonliving Matter. *Acc. Chem. Res.* **45**, 2131–2141 (2012).
4. Cronin, L. & Walker, S. I. Beyond prebiotic chemistry. *Science* **352**, 1174–1175 (2016).
5. Dzieciol, A. J. & Mann, S. Designs for life: protocell models in the laboratory. *Chem Soc Rev* **41**, 79–85 (2012).
6. Poudyal, R. R., Pir Cakmak, F., Keating, C. D. & Bevilacqua, P. C. Physical Principles and Extant Biology Reveal Roles for RNA-Containing Membraneless Compartments in Origins of Life Chemistry. *Biochemistry* **57**, 2509–2519 (2018).
7. Toparlak, O. D. & Mansy, S. S. Progress in synthesizing protocells. *Exp. Biol. Med.* **244**, 304–313 (2019).
8. Kurihara, K. *et al.* A recursive vesicle-based model protocell with a primitive model cell cycle. *Nat Commun* **6**, 8352 (2015).
9. Blain, J. C. & Szostak, J. W. Progress Toward Synthetic Cells. *Annu. Rev. Biochem.* **83**, 615–640 (2014).
10. Hanczyc, M. M., Fujikawa, S. M. & Szostak, J. W. Experimental Models of Primitive Cellular Compartments: Encapsulation, Growth, and Division. *Science* **302**, 618–622 (2003).
11. Monnard, P.-A. & Deamer, D. W. Membrane self-assembly processes: Steps toward the first cellular life. *Anat. Rec.* **268**, 196–207 (2002).
12. Litschel, T. *et al.* Freeze-thaw cycles induce content exchange between cell-sized lipid vesicles. *New J. Phys.* **20**, 055008 (2018).
13. Koga, S., Williams, D. S., Perriman, A. W. & Mann, S. Peptide–nucleotide microdroplets as a step towards a membrane-free protocell model. *Nat. Chem.* **3**, 720–724 (2011).
14. Drobot, B. *et al.* Compartmentalised RNA catalysis in membrane-free coacervate protocells. *Nat. Commun.* **9**, 3643 (2018).
15. Poudyal, R. R. *et al.* Template-directed RNA polymerization and enhanced ribozyme catalysis inside membraneless compartments formed by coacervates. *Nat. Commun.* **10**, 490 (2019).
16. Nakashima, K. K., Baaij, J. F. & Spruijt, E. Reversible generation of coacervate droplets in an enzymatic network. *Soft Matter* **14**, 361–367 (2018).
17. Love, C. *et al.* Reversible pH-Responsive Coacervate Formation in Lipid Vesicles Activates Dormant Enzymatic Reactions. *Angew. Chem. Int. Ed.* **59**, 5950–5957 (2020).
18. Boeynaems, S. *et al.* Protein Phase Separation: A New Phase in Cell Biology. *Trends Cell Biol.* **28**, 420–435 (2018).
19. Shin, Y. & Brangwynne, C. P. Liquid phase condensation in cell physiology and disease. *Science* **357**, eaaf4382 (2017).

20. Banani, S. F., Lee, H. O., Hyman, A. A. & Rosen, M. K. Biomolecular condensates: organizers of cellular biochemistry. *Nat. Rev. Mol. Cell Biol.* **18**, 285–298 (2017).
21. Yin, Y. *et al.* Non-equilibrium behaviour in coacervate-based protocells under electric-field-induced excitation. *Nat. Commun.* **7**, 10658 (2016).
22. Perry, S. L. *et al.* Chirality-selected phase behaviour in ionic polypeptide complexes. *Nat. Commun.* **6**, (2015).
23. Aumiller, W. M. & Keating, C. D. Phosphorylation-mediated RNA/peptide complex coacervation as a model for intracellular liquid organelles. *Nat. Chem.* **8**, 129–137 (2016).
24. Murthy, A. C. *et al.* Molecular interactions underlying liquid–liquid phase separation of the FUS low-complexity domain. *Nat. Struct. Mol. Biol.* **26**, 637–648 (2019).
25. Martin, E. W. *et al.* Valence and patterning of aromatic residues determine the phase behavior of prion-like domains. *Science* **367**, 694–699 (2020).
26. Gomes, E. & Shorter, J. The molecular language of membraneless organelles. *J. Biol. Chem.* **294**, 7115–7127 (2019).
27. Reches, M. & Gazit, E. Formation of Closed-Cage Nanostructures by Self-Assembly of Aromatic Dipeptides. *Nano Lett.* **4**, 581–585 (2004).
28. Adler-Abramovich, L. & Gazit, E. The physical properties of supramolecular peptide assemblies: from building block association to technological applications. *Chem Soc Rev* **43**, 6881–6893 (2014).
29. Chen, C., Liu, K., Li, J. & Yan, X. Functional architectures based on self-assembly of bio-inspired dipeptides: Structure modulation and its photoelectronic applications. *Adv. Colloid Interface Sci.* **225**, 177–193 (2015).
30. Yuan, C. *et al.* Nucleation and Growth of Amino Acid and Peptide Supramolecular Polymers through Liquid–Liquid Phase Separation. *Angew. Chem. Int. Ed.* **58**, 18116–18123 (2019).
31. Brady, J. P. *et al.* Structural and hydrodynamic properties of an intrinsically disordered region of a germ cell-specific protein on phase separation. *Proc. Natl. Acad. Sci.* **114**, E8194–E8203 (2017).
32. Sprakel, J., Besseling, N. A. M., Cohen Stuart, M. A. & Leermakers, F. A. M. Phase behavior of flowerlike micelles in a SCF cell model. *Eur. Phys. J. E* **25**, 163–173 (2008).
33. Srivastava, S. *et al.* Gel phase formation in dilute triblock copolyelectrolyte complexes. *Nat. Commun.* **8**, 14131 (2017).
34. Zhang, X., Malhotra, S., Molina, M. & Haag, R. Micro- and nanogels with labile crosslinks – from synthesis to biomedical applications. *Chem. Soc. Rev.* **44**, 1948–1973 (2015).
35. Bungenberg de Jong, H. G. & Kruyt, H. R. Coacervation (Partial miscibility in colloid systems). *Proc. Neth. Acad. Sci.* **32**, 849–856.
36. Kaminker, I. *et al.* Simple peptide coacervates adapted for rapid pressure-sensitive wet adhesion. *Soft Matter* **13**, 9122–9131 (2017).
37. Gutierrez, J. M. P., Hinkley, T., Taylor, J. W., Yanev, K. & Cronin, L. Evolution of oil droplets in a chemorobotic platform. *Nat. Commun.* **5**, ncomms6571 (2014).
38. Tena-Solsona, M., Wanzke, C., Riess, B., Bausch, A. R. & Boekhoven, J. Self-selection of dissipative assemblies driven by primitive chemical reaction networks. *Nat. Commun.* **9**, 2044 (2018).
39. Cashman, T. J. & Linton, B. R. β -Sheet Hydrogen Bonding Patterns in Cystine Peptides. *Org. Lett.* **9**, 5457–5460 (2007).
40. Biancalana, M., Makabe, K., Koide, A. & Koide, S. Molecular Mechanism of Thioflavin-T Binding to the Surface of β -Rich Peptide Self-Assemblies. *J. Mol. Biol.* **385**, 1052–1063 (2009).
41. Nott, T. J., Craggs, T. D. & Baldwin, A. J. Membraneless organelles can melt nucleic acid duplexes and act as biomolecular filters. *Nat. Chem.* **8**, 569–575 (2016).
42. Sokolova, E. *et al.* Enhanced transcription rates in membrane-free protocells formed by coacervation of cell lysate. *Proc. Natl. Acad. Sci.* **110**, 11692–11697 (2013).
43. Luppi, G. *et al.* Dipeptide-Catalyzed Asymmetric Aldol Condensation of Acetone with (N-Alkylated) Isatins. *J. Org. Chem.* **70**, 7418–7421 (2005).
44. Springsteen, G., Yerabolu, J. R., Nelson, J., Rhea, C. J. & Krishnamurthy, R. Linked cycles of oxidative decarboxylation of glyoxylate as protometabolic analogs of the citric acid cycle. *Nat. Commun.* **9**, 91 (2018).
45. Huerta, E., van Genabeek, B., Stals, P. J. M., Meijer, E. W. & Palmans, A. R. A. A Modular Approach to Introduce Function into Single-Chain Polymeric Nanoparticles. *Macromol. Rapid Commun.* **35**, 1320–1325 (2014).
46. Dirksen, A., Dirksen, S., Hackeng, T. M. & Dawson, P. E. Nucleophilic Catalysis of Hydrazone Formation and Transimination: Implications for Dynamic Covalent Chemistry. *J. Am. Chem. Soc.* **128**, 15602–15603 (2006).
47. Li, J. *et al.* Determination of residual phenylhydrazines in drug substances by high-performance liquid chromatography with pre-column derivatization. *Anal. Methods* **11**, 6146–6152 (2019).
48. Frederix, P. W. J. M. *et al.* Exploring the sequence space for (tri-)peptide self-assembly to design and discover new hydrogels. *Nat. Chem.* **7**, 30–37 (2015).
49. Serrano-Luginbühl, S., Ruiz-Mirazo, K., Ostaszewski, R., Gallou, F. & Walde, P. Soft and dispersed interface-rich aqueous systems that promote and guide chemical reactions. *Nat. Rev. Chem.* **2**, 306–327 (2018).

Methods

Synthesis. All peptide derivatives were synthesised via the solution-phase synthesis methods. Full details of the synthesis and characterisations are given in the supporting information.

Coacervation. The lyophilized powder of dipeptide derivatives was dissolved in milli-Q water. The pH of the homogeneous solution of peptide derivatives was in the range of 5 to 6 depending on the concentration of the peptide. The coacervation/aggregation was triggered by increasing the pH to 7 using 1 μ l of 0.2 M NaOH solution or 5 μ l of 100 mM phosphate/Tris/TEAB buffer for each 100 μ L solution of peptide. The milky colour appeared immediately and coacervation was confirmed by brightfield microscopy (Olympus IX71 inverted microscope).

Turbidity. All turbidity-based titrations were performed on a Tecan Spark multimode plate reader with a built-in spectrophotometer and automated injector. We use turbidity as an indicator of LLPS for samples in which liquid droplets have been confirmed by optical microscopy. We used 600 nm as the wavelength for all turbidity measurements, and all measurements were performed at room temperature ($21 \pm 2^\circ\text{C}$), unless stated otherwise. Titrations were carried out in triplicate and the titrant concentration was chosen such that the added volume did not exceed 10% of the original volume, except for acetonitrile and L-phenylalanine methyl ester (Phe-OMe) titrations. Turbidity was recorded after shaking the sample for 5 seconds following each addition. A well with the same volume of buffer was used as blank.

Partitioning experiments. For partitioning of guest molecules we used a 1 mg/mL stock solution of FFssFF at pH<6. We prepared 1 mM stock solutions of the dye molecules, 10 μ M stock solutions of ssDNA-FAM (140 ng/ μ L), ssRNA-Cy5 (85 ng/ μ L) and RNA hairpin (100 ng/ μ L), and a saturated solution of protoporphyrin IX in Milli-Q water. 20 μ L of FFssFF stock solution was mixed with 2 μ L of a 100 mM buffer solution pH 7.5 (Tris) to induce coacervation. After 1 minute, 2 μ L of the dye stock solutions or 1 μ L of the nucleic acid stock solutions was added and mixed with the coacervates by pipetting. The mixtures were incubated for 30 minutes, and after incubation 10 μ l of the mixture was applied to cover glass (No. 1.5H) and imaged directly using a CSU X-1 Yokogawa spinning disc confocal on an Olympus IX81 inverted microscope, or a Leica TCS Sp8X confocal microscope (HC PL APO 100x/1.40 (oil) CS2 objective).

Microreactor experiment. We performed two chemical reactions to test the catalytic activity of FFssFF coacervates.

(1) The aldol reaction between 4-nitrobenzaldehyde and cyclohexanone was performed with and without FFssFF coacervates at pH 9. Fresh stock solutions of 4-nitrobenzaldehyde (1.0 M) and cyclohexanone (1.0 M) in DMSO-*d*₆ and FFssFF (1 mg/mL) in D₂O were prepared. To induce coacervation, 2 μ L of NaOD (0.87 M in D₂O) was added to 1 mL of the peptide solution, followed by the addition of 5 μ L of dioxane in D₂O (2 M) as internal standard, and 10 μ L of 4-nitrobenzaldehyde. All components were mixed well in a 5 mm NMR tube. A pre-scan was performed to calculate the exact concentration of aldehyde in the reaction mixture. Then, 20 μ L of cyclohexanone was added into the NMR tube to initiate the aldol reaction, everything was mixed and ¹H NMR spectra of the reaction mixture were recorded at regular time intervals.

(2) Hydrazone formation between phenylhydrazine and 4-nitrobenzaldehyde was carried out with and without FFssFF coacervates at pH 8.5, which was set using 10 mM phosphate buffer saline (with 137 mM NaCl and 2.7 mM KCl). Fresh stock solutions of 4-nitrobenzaldehyde (300 mM), and phenylhydrazine (60 mM) were prepared in DMF, and a stock solution of FFssFF (2 mg/mL) was prepared in milliQ water. Coacervation was induced by mixing 300 μ L of the FFssFF solution with 300 μ L phosphate buffer saline (10 mM, pH 8.5). 600 μ L of that suspension was mixed with 2 μ L of the phenylhydrazine solution and 2 μ L of the 4-nitrobenzaldehyde solution, by vortexing. Aliquots (50 μ L) were taken from the reaction mixture every 10 minutes, and the coacervates were dissolved by mixing with an equal volume of acetonitrile, yielding a clear solution. Absorption spectra of the samples were recorded on a Jasco V-630 UV-Vis spectrophotometer. The remaining detail about the control experiments of addition reactions is in the supporting information.